

Phase Field Crystal Study of Symmetric Tilt Grain Boundaries of Iron

A. Jaatinen^{1,2}, C. V. Achim³, K. R. Elder⁴, T. Ala-Nissila^{1,5}

*We apply the phase field crystal model to study the structure and energy of symmetric tilt grain boundaries of bcc iron in 3D. The parameters for the model are obtained by using a recently developed eight-order fitting scheme [A. Jaatinen et al., Phys. Rev. B **80**, 031602 (2009)]. The grain boundary free energies we obtain from the model are in good agreement with previous results from molecular dynamics simulations and experiments.*

1 Introduction

One of the challenges in modern computational materials science is being able to access phenomena that take place on different time and length scales. Recently, a new model called the phase field crystal (PFC) model has been constructed that describes phenomena taking place on atomic length scale but diffusive time scales (Elder et al., 2002), the combination of which has been inaccessible for molecular dynamics (MD) simulations using present day computers. The PFC method is able to achieve this combination of scales by replacing the individual atoms in MD simulations by a continuous field that exhibits the periodic nature of the underlying atomic lattice in the solid phase, but evolves in diffusive time scales. As the original formulation of the PFC model relies on a phenomenologically constructed free energy functional, it has proven challenging to quantitatively relate the parameters that enter the PFC model to the properties of real materials. In a recent study, we have shown how the PFC model can be modified in such a way that many relevant material properties can be included in the PFC free energy, while still conserving most of the computational simplicity of the model (Jaatinen et al., 2009). This can be achieved using the so-called Eighth Order fitting (EOF) scheme. In the present work, we use the EOF-PFC model to study the energy of symmetrically tilted grain boundaries of bcc iron near its melting point. Results of our calculations will provide an independent theoretical prediction for the grain boundary energy of iron near its melting point. Perhaps more importantly, they also provide indication on whether the EOF scheme is a good candidate for future studies of grain boundary related phenomena, such as grain boundary premelting (Berry et al., 2008; Mellenthin et al., 2008) and nanocrystalline deformation (Elder and Grant, 2004; Stefanovic et al., 2009), with the PFC model.

2 Model

The phase field crystal (PFC) model describes crystallization phenomena and has been applied to many different problems in materials science. Originally, the model was phenomenologically postulated in the spirit of the Ginzburg-Landau theory by Elder et al. (2002). The model consists of an order parameter field that is driven by dissipative, conserved dynamics to minimize a free energy functional, whose ground state exhibits a periodic structure commensurate with the crystal symmetry of interest. More specifically, the deterministic equation of motion for the locally conserved order parameter field $n(\mathbf{r})$ in these models is given by

$$\frac{\partial n}{\partial t} = M \nabla^2 \frac{\delta F}{\delta n}, \quad (1)$$

where M is mobility and F is free energy of the system as a functional of the field $n(\vec{r}, t)$. The most usual choice of a free energy functional for PFC studies is the form derived by Swift and Hohenberg (1977) for a study of convective instabilities. Here we briefly describe the procedure suggested by Jaatinen et al. (2009) for obtaining a free energy that is capable of describing body-centered cubic materials from a fundamental basis.

Derivation of our free energy starts from the classical density-functional theory (DFT) of freezing, first pioneered by Ramakrishnan and Yussouff (1979). The simplest free energy used in DFT of freezing studies can be obtained by expanding the excess (over ideal gas) contribution to the free energy around a uniform reference density ρ_0 ,

leading to

$$\frac{\Delta F[n(\mathbf{r})]}{k_B T \rho_0} = \int d\mathbf{r} [(1 + n(\mathbf{r})) \ln(1 + n(\mathbf{r})) - n(\mathbf{r})] - \frac{1}{2} \int d\mathbf{r} \int d\mathbf{r}' n(\mathbf{r}) C(|\mathbf{r} - \mathbf{r}'|) n(\mathbf{r}'), \quad (2)$$

where ΔF is the free energy difference between a given state and the reference, $k_B T$ is the thermal energy and the order-parameter field n is related to the ensemble-averaged one-particle density $\rho(\mathbf{r})$ through $n(\mathbf{r}) = (\rho(\mathbf{r}) - \rho_0)/\rho_0$. The function C entering Eq. (2) is the two-body direct correlation function (DCF) of the reference liquid, which is related to the total pair correlation function, and thus structure factor of the liquid through the well-known Ornstein-Zernike relation.

In principle it is possible to use Eq. (2) for PFC studies; however, in practice solutions of this equation are very sharply peaked in space (around atomic lattice positions) which restricts numerical calculations to very small systems. To overcome this difficulty, we make two approximations. Firstly, the non-local part of F is simplified by expanding the DCF in k -space up to eighth order as

$$C(k) \approx C(k_m) - \Gamma \left(\frac{k_m^2 - k^2}{k_m^2} \right)^2 - E_B \left(\frac{k_m^2 - k^2}{k_m^2} \right)^4, \quad (3)$$

where the parameter k_m is the position of the first maximum in the original DCF, and Γ and E_B are chosen such that the expansion reproduces the position, height and curvature of the first maximum, and the $k = 0$ value of the original DCF. This is achieved by choosing

$$\Gamma = -\frac{k_m^2 C''(k_m)}{8}, \quad (4)$$

where primes denote derivatives with respect to k , and

$$E_B = C(k_m) - C(0) - \Gamma. \quad (5)$$

As shown by Jaatinen et al. (2009), this eighth order expansion provides an excellent fit from $k = 0$ to the first peak in $C(k)$ in the case of iron. However, for the density oscillations whose wave vector corresponds to a k larger than k_m , the expanded free energy now results in a significantly larger free energy penalty, thus reducing stability of the solid phase. In order to partly correct this error, and to further simplify the mathematical form of the free energy, the local part is expanded in a fourth order power series as

$$(1 + n) \ln(1 + n) - n \approx \frac{1}{2} n^2 - \frac{a}{6} n^3 + \frac{b}{12} n^4. \quad (6)$$

The coefficient $1/2$ for the second order term in this series is obtained from a Taylor series in order to conserve the linear stability of the model. For the third and fourth order terms we have included constants a and b , which are chosen such that the solid will stabilize in the model, with the correct amplitude of density fluctuations corresponding to the first star of reciprocal lattice vectors, u_s . This is approximately achieved by choosing them as

$$a = \frac{3}{2S(k_m)u_s}; \quad b = \frac{4}{30S(k_m)u_s^2}, \quad (7)$$

where $S(k_m) = (1 - C(k_m))^{-1}$ is height of the first peak in the structure factor of the reference liquid (Jaatinen et al., 2009). With these approximations, the free energy finally becomes

$$\frac{\Delta F[n(\mathbf{r})]}{k_B T \rho_0} = \int d\mathbf{r} \left[\frac{n(\mathbf{r})}{2} \left(1 - C(k_m) + \Gamma \left(\frac{k_m^2 + \nabla^2}{k_m^2} \right)^2 + E_B \left(\frac{k_m^2 + \nabla^2}{k_m^2} \right)^4 \right) n(\mathbf{r}) - \frac{a}{6} n(\mathbf{r})^3 + \frac{b}{12} n(\mathbf{r})^4 \right]. \quad (8)$$

In our previous study we fitted the parameters of the current model with molecular dynamics simulation data from Wu and Karma (2007), complemented by experimental data from Itami and Shimoji (1984) and Jimbo and Cramb (1993), for iron. The resulting model parameters are $k_m = 2.985 \text{ \AA}^{-1}$, $C(k_m) = 0.668$, $\Gamma = 11.583$ and $E_B = 38.085$ for the DCF part, and $a = 0.6917$ and $b = 0.08540$ for the non-linear part. The reference temperature and density, necessary for converting model results into SI units are $T = 1772 \text{ K}$ and $\rho_0 = 0.0801 \text{ \AA}^{-3}$. We have also shown that with these parameters, the model produces very reasonable predictions for bulk modulus, solid-liquid coexistence gap and low index surface free energies. (Jaatinen et al., 2009) In the next section, we will show that this model is also capable of describing grain boundaries in iron.

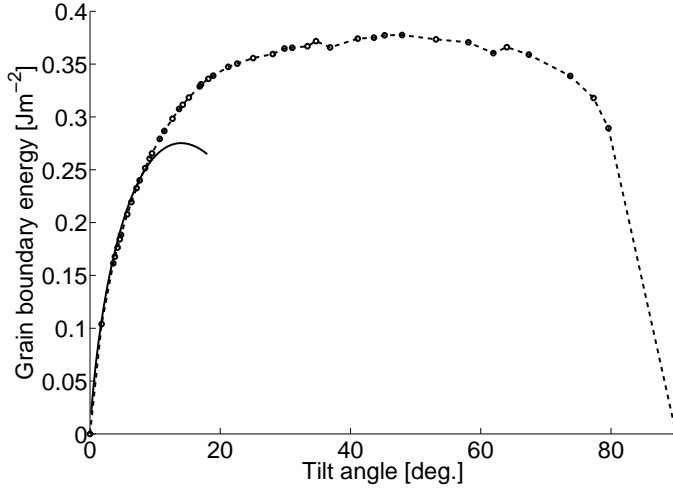


Figure 1: Grain boundary free energy as a function of the misorientation angle θ when the tilt axis is in the $\langle 100 \rangle$ direction. Solid line shows the best fit to the Read-Shockley equation at small tilt angles. Dashed line is a guide to the eye.

3 Grain boundaries

Using the model and parameters described in the previous section, we have studied the symmetrically tilted grain boundaries of iron. Three choices of tilting axis, $\langle 100 \rangle$, $\langle 110 \rangle$ and $\langle 111 \rangle$, were studied. The calculations were performed at a density of $(\rho - \rho_0)/\rho_0 = 0.030$, which is just above the density of the solid at coexistence. A density close to the solid-liquid coexistence was chosen due to the fact that the model parameters have been obtained to reproduce the selected properties of iron close to its melting point (Jaatinen et al., 2009).

First, we have found the lattice constant a of the bcc phase that minimizes the free energy at the density in question. Then, a computational box of dimensions (L_x, L_y, L_z) , and periodic boundary conditions in all directions was initialized by using the one-mode approximation,

$$n(\mathbf{r}) = n_0 + (1 + n_0)4u [\cos(qx) \cos(qy) + \cos(qx) \cos(qz) + \cos(qy) \cos(qz)], \quad (9)$$

where $q = 2\pi/a_{bcc}$, a_{bcc} being the lattice spacing, and u is the amplitude of density fluctuations. First, a rotation to the one-mode approximation was applied such that the tilt axis was parallel to the z axis of the computational box. Then, in the region $x = 0 \dots L_x/2$, the one-mode approximation was rotated in the (x, y) plane by an angle $-\theta/2$, and in the region $x = L_x/2 \dots L_x$ by an angle $\theta/2$, creating two symmetrically tilted grain boundaries, located at $x = 0$ and $x = L_x/2$, with a tilting angle θ . The tilting angles θ and box dimensions (L_x, L_y, L_z) were chosen such that the periodic pattern of the lattice continues smoothly over the periodic boundaries in the y and z directions, and an integer number of atomic planes was placed between the two grain boundaries in the system. The system size in the direction of the tilting axis, L_z , was chosen to be the closest distance between two similar atomic planes in the z -direction. In the perpendicular directions, L_x and L_y were varied from case to case, such that for small angles, the simulation box contained several thousands of maxima, while for large angle calculations, only hundreds of maxima were required, due to the smaller spacing between dislocations at the boundary.

In order to find the minimum energy of the system with the grain boundaries, we have numerically integrated Eq. (1) until convergence, using the semi-implicit operator splitting method of Tegze et al. (2009). The Laplace operator is discretized in k -space as $\Delta_{\mathbf{k}} = -k^2$. Grain boundary free energy per unit area, E_{gb} , is then obtained from

$$E_{gb} = L_z \frac{f - f_b}{2}, \quad (10)$$

where f is the average free energy density of the final configuration, and f_b is free energy density of a non-rotated system.

Fig. 1 shows the results of our grain boundary free energy calculations, and Fig. 2 shows three example final configurations for the $\langle 100 \rangle$ case. As in previous studies utilizing the original PFC free energy functional (Elder et al.,

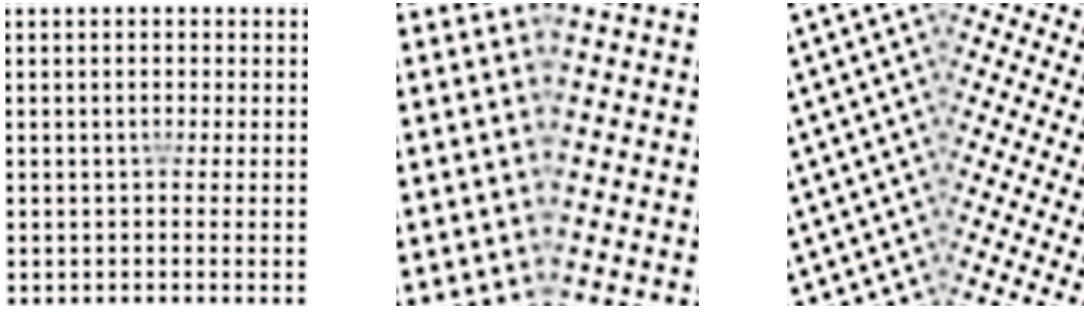


Figure 2: Example final configurations from the $\langle 100 \rangle$ case. The gray scale in these figures corresponds to $n(x, y, 0)$. On the left, we show the low-angle $\text{bcc}(0\ 64\ 1)\langle 100 \rangle \Sigma 40975$ ($\theta = 1.79^\circ$) boundary, where one clearly sees the individual dislocation. The middle figure shows a large angle $\text{bcc}(051)\langle 100 \rangle \Sigma 13$ ($\theta = 22.62^\circ$) boundary, and the figure on the right shows the $\text{bcc}(031)\langle 100 \rangle \Sigma 5$ ($\theta = 36.87^\circ$), for which a small energy cusp was observed.

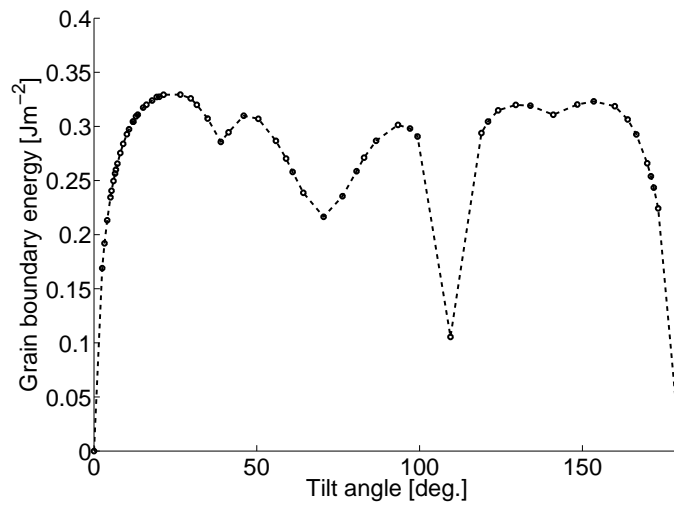


Figure 3: Grain boundary free energy as a function of the misorientation angle θ when the tilt axis is in the $\langle 110 \rangle$ direction. Dashed line is a guide to the eye.

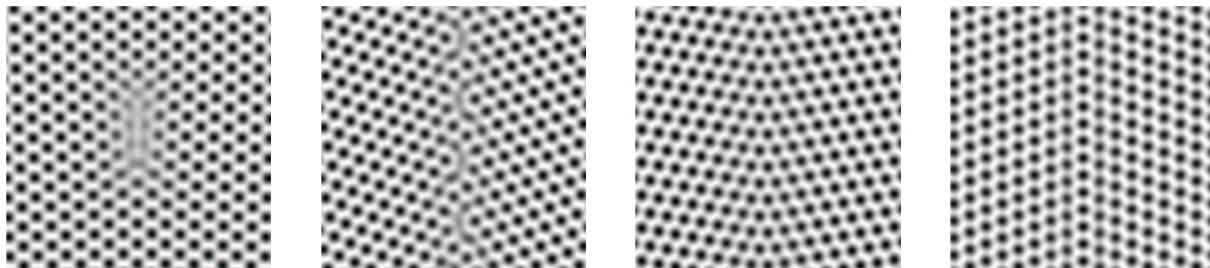


Figure 4: Example final configurations from the $\langle 110 \rangle$ case, with the gray scale corresponding to $n(x, y, 0)$. From left to right, the corresponding grain boundaries are $\text{bcc}(32\ 32\ 1)\langle 110 \rangle \Sigma 2049$ ($\theta = 2.53^\circ$), $\text{bcc}(331)\langle 110 \rangle \Sigma 19$ ($\theta = 26.52^\circ$), $\text{bcc}(332)\langle 110 \rangle \Sigma 11$ ($\theta = 50.47^\circ$) and $\text{bcc}(112)\langle 110 \rangle \Sigma 3$ ($\theta = 109.47^\circ$).

2002; Elder and Grant, 2004; Mellenthin et al., 2008), we find that for small angles the grain boundary energy closely follows the expression by Read and Shockley (1950),

$$E_{gb} = E_0 \theta (A - \ln(\theta)), \quad (11)$$

where E_0 is an energy scale that depends on elastic properties of the material studied, and the constant A depends on the dislocation core energy. In addition, both of these constants depend on the orientation of the grain boundary. In the present work, as we have not developed numerical tools for quantifying all the properties that enter the expressions for E_0 and A (Read and Shockley, 1950), we have chosen to treat them as fitting parameters. The best fit to the current data gives $E_0 = 1.1271 \text{ Jm}^{-2}$ and $A = -0.41$.

For large values of θ , the changes in E_{gb} are moderate, with the maximum value being 0.377 Jm^{-2} . By close inspection of Fig. 1 one can distinguish small energy cusps at angles corresponding to bcc(031) $\langle 100 \rangle \Sigma 5$ ($\theta = 36.87^\circ$) and bcc(053) $\langle 100 \rangle \Sigma 17$ ($\theta = 61.93^\circ$) grain boundary planes. Both of these energy cusps correspond to a low coincidence site lattice (CSL) Σ . However, for the other low- Σ grain boundaries, for example the bcc(021) $\langle 100 \rangle \Sigma 5$ ($\theta = 53.13^\circ$), no such cusps were observed. More generally, we do not observe any clear correlation between the CSL Σ and energies of large angle grain boundaries. Thus, our results do not agree with Zhang et al. (2005) who found, using molecular statics with modified analytical embedded atom method, that the energy of symmetrically tilted grain boundaries in iron increases with increasing Σ . Our results agree much better with Shibuta et al. (2008) who have performed molecular dynamics simulations with Finnis-Sinclair potential to calculate the energies of different symmetric tilt boundaries of iron in different temperatures. Their results are qualitatively (but not quantitatively) very similar to ours, and they also observe the small energy cusp at bcc(031) $\langle 100 \rangle \Sigma 5$ present in our results as well. However, unlike in our results, Shibuta et al. (2008) observe another small energy cusp at bcc(021) $\langle 100 \rangle \Sigma 5$. The cusp we observe at bcc(053) $\langle 100 \rangle \Sigma 17$ is not present in their results.

Results of our grain boundary free energy calculations for the $\langle 110 \rangle$ case are shown in Fig. 3, and example final configurations for this case are shown in Fig. 4. The low-angle behavior of E_{gb} vs. θ is qualitatively very similar to the $\langle 100 \rangle$ case, but at large angles, interesting features are observed. There is a deep minimum corresponding to bcc(112) $\langle 110 \rangle \Sigma 3$ ($\theta = 109.47^\circ$), which is a twin boundary. The grain boundary energy in this minimum is only approximately third of the maximum values observed. Other clear local minima are observed at bcc(221) $\langle 110 \rangle \Sigma 9$ ($\theta = 38.94^\circ$), bcc(111) $\langle 110 \rangle \Sigma 3$ ($\theta = 70.53^\circ$) and bcc(114) $\langle 110 \rangle \Sigma 9$ ($\theta = 141.06^\circ$). Thus for $\langle 110 \rangle$ grain boundaries all angles with $\Sigma < 10$ correspond to a local minimum in grain boundary energy. However, as in the $\langle 100 \rangle$ case, we do not find a more general correlation between Σ and E_{gb} , as can be seen from Fig 5, where we plot E_{gb} vs. Σ for the $\langle 110 \rangle$ case. In comparison of our results with Shibuta et al. (2008), we find that our depth of the bcc(112) $\langle 110 \rangle \Sigma 3$ minimum is in an excellent agreement with their work. However, their bcc(221) $\langle 110 \rangle \Sigma 9$ minimum is much less pronounced than in our work, and the remaining two of the local minima, that we observed, were not observed in their study at all. Instead, they observe a small energy cusp at bcc(554) $\langle 110 \rangle \Sigma 33$ ($\theta = 58.99^\circ$), which we did not find anomalous.

Results for the case where tilting axis is in the $\langle 111 \rangle$ direction are shown in Fig. 6. In this case, the energy increases with increasing misorientation, without any noteworthy energy cusps, until reaching a maximum value at $\theta = 32.20^\circ$. When further increasing θ from that maximum, the grain boundary decreases, as the orientation gets closer to the partial matching at $\theta = 60^\circ$. Finally, at $\theta = 60^\circ$ (i.e. bcc(121) $\langle 111 \rangle \Sigma 3$) the grain boundary energy is 0.357 Jm^{-2} , which is approximately 30 % of the maximum value. The place of the maximum energy, magnitude of the $\theta = 60^\circ$ value compared to the maximum, and the absence of energy cusps agree very well with the molecular dynamics results of Shibuta et al. (2008).

Experimentally, the large angle grain boundary energy of δ iron has been determined to be 0.468 Jm^{-2} (Murr, 1975), in good agreement with our maximum value. It is also worthwhile noting that the agreement of our results with Murr (1975) for the ratio of large angle grain boundary energy to the solid-liquid surface free energy is even better: $E_{gb}/\sigma_{s-l} \approx 2.16$ in the present model (solid-liquid surface energy from Jaatinen et al. (2009)), where the values from Murr (1975) give $E_{gb}/\sigma_{s-l} \approx 2.29$. When comparing our values for grain boundary energies with the results of the previously mentioned atomistic calculations, we observe that the grain boundary energies obtained by Zhang et al. (2005) are of the order of several Joules per square meter, being significantly higher than the values reported here or those reported by by Shibuta et al. (2008). It should be noted that the calculations of Zhang et al. (2005) were conducted at absolute zero temperature, not near the melting point, which perhaps explains this discrepancy. The grain boundary energies reported by Shibuta et al. (2008), on the other hand, reach a maximum of approximately 1.6 Jm^{-2} at moderate temperatures, rising to approximately 2.4 Jm^{-2} close to the melting point. A likely reason for our grain boundary energies being closer to the experimental values than those

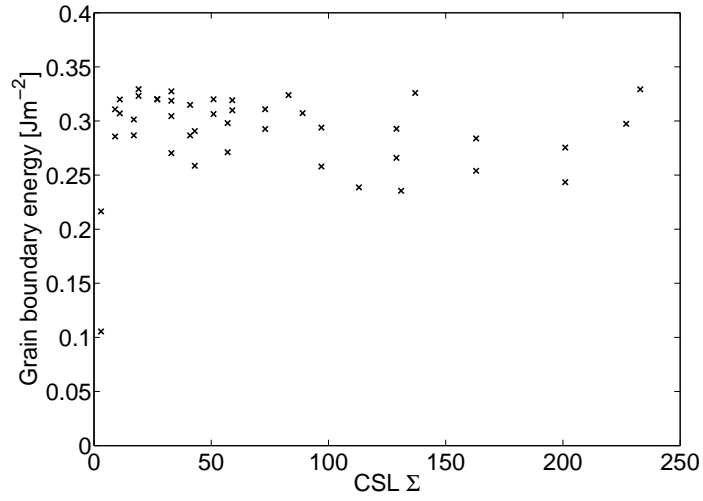


Figure 5: Grain boundary free energy as a function of the coincidence site lattice Σ when the tilt axis is in the $\langle 110 \rangle$ direction.

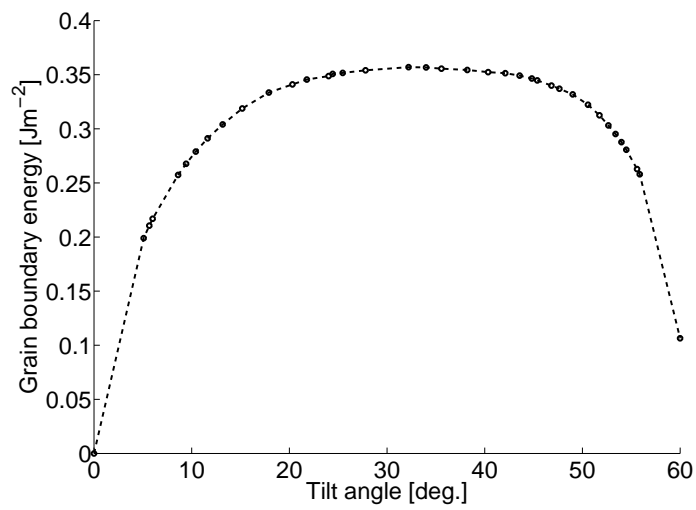


Figure 6: Grain boundary free energy as a function of the misorientation angle θ when the tilt axis is in the $\langle 111 \rangle$ direction. Dashed line is a guide to the eye.

of Shibuta et al. (2008) is that we are, in accordance to the experimentalists, actually measuring the grain boundary *free energy*, unlike Shibuta et al. (2008) who only measure the excess energy of creating a grain boundary, without taking into account the entropic part of the free energy.

4 Conclusion

We have applied the recently established EOF-PFC model to study the structure and energy of symmetric tilt grain boundaries in iron, with the axis of rotation parallel to $\langle 100 \rangle$ and $\langle 110 \rangle$ directions. For small misorientation angles, we found that the grain boundary energy increases with increasing misorientation, in agreement with the Read-Shockley equation. For large misorientation angles, we observed local minima in the grain boundary energy vs. misorientation curve, many of which have been observed in molecular dynamics simulations as well. The local minima are associated with low values of the coincidence site lattice Σ , but no general correlation between Σ and the grain boundary energy was found. In general, the qualitative agreement between present results and previous MD results at finite temperature was found to be good. Quantitatively, the agreement of our result with an experimental value for the large angle grain boundary energy is better than that from the MD. As our phase field crystal results agree well with previous MD study of grain boundaries in iron, and an experimental large angle grain boundary energy, they may even be considered an independent prediction for the angular dependence of grain boundary energy in iron. More importantly, they show the potential of the EOF-PFC in modeling materials properties where grain boundaries play an important role.

5 Acknowledgements

This work was supported in part by the Academy of Finland through its Center of Excellence COMP grant, Tekes through its MASIT33 project, and joint funding under EU STREP Grant No. 016447 MagDot and NSF DMR Grant No. 0502737. K.R.E. acknowledges support from NSF under Grant No. DMR-0906676.

References

- Berry, J.; Elder, K. R.; Grant, M.: Melting at dislocations and grain boundaries: A phase field crystal study. *Phys. Rev. B*, 77, (2008), 224114.
- Elder, K. R.; Grant, M.: Modeling elastic and plastic deformations in nonequilibrium processing using phase field crystals. *Phys. Rev. E*, 70, (2004), 051605.
- Elder, K. R.; Katakowski, M.; Haataja, M.; Grant, M.: Modeling elasticity in crystal growth. *Phys. Rev. Lett.*, 88, (2002), 245701.
- Itami, T.; Shimoji, M.: Application of simple model theories to thermodynamic properties of liquid transition metals. *J. Phys. F: Met. Phys.*, 14, (1984), L15–L20.
- Jaatinen, A.; Achim, C. V.; Elder, K. R.; Ala-Nissila, T.: Thermodynamics of bcc metals in phase-field-crystal models. *Phys. Rev. E*, 80, (2009), 031602.
- Jimbo, I.; Cramb, A. W.: The density of liquid iron-carbon alloys. *Metall. Mater. Trans. B*, 24, (1993), 5–10.
- Mellenthin, J.; Karma, A.; Plapp, M.: Phase-field crystal study of grain-boundary premelting. *Phys. Rev. B*, 78, (2008), 184110.
- Murr, L. E.: *Interfacial Phenomena in Metals and Alloys*. Addison Wesley, New York (1975).
- Ramakrishnan, T. V.; Yussouff, M.: First-principles order-parameter theory of freezing. *Phys. Rev. B*, 19, (1979), 2775–2794.
- Read, W. T.; Shockley, W.: Dislocation models of crystal grain boundaries. *Phys. Rev.*, 78, (1950), 275 – 289.
- Shibuta, Y.; Takamoto, S.; Suzuki, T.: A molecular dynamics study of the energy and structure of the symmetric tilt boundary of iron. *ISIJ Int.*, 48, (2008), 1582–1591.
- Stefanovic, P.; Haataja, M.; Provatas, N.: Phase-field crystal study of deformation and plasticity in nanocrystalline materials. *Phys. Rev. E*, 80, (2009), 046107.

Swift, J.; Hohenberg, P. C.: Hydrodynamic fluctuations at the convective instability. *Phys. Rev. A*, 15, (1977), 319–328.

Tegze, G.; Bansel, G.; Tóth, G. I.; Pusztai, T.; Fan, Z.; Gránásy, L.: Advanced operator splitting-based semi-implicit spectral method to solve the binary phase-field crystal equations with variable coefficients. *J. Comp. Phys.*, 228, (2009), 1612–1623.

Wu, K.-A.; Karma, A.: Phase-field crystal modeling of equilibrium bcc-liquid interfaces. *Phys. Rev. B*, 76, (2007), 184107.

Zhang, J.-M.; Huang, Y.-H.; Wu, X.-J.; Xu, K.-W.: Energy calculation for symmetric tilt grain boundaries in iron. *Appl. Surf. Sci.*, 252, (2005), 4936–4942.

Address: ¹Department of Applied Physics and COMP Center of Excellence, Helsinki University of Technology, P.O. Box 1100, Helsinki FI-02015 TKK, Finland

²Department of Materials Science and Engineering, Helsinki University of Technology, P.O. Box 6200, Helsinki FIN-02015 TKK, Finland

³Institut für Theoretische Physik II: Weiche Materie, Heinrich-Heine-Universität, Universitätsstrasse 1, D-40225 Düsseldorf, Germany

⁴Department of Physics, Oakland University, Rochester, Michigan 48309-4487, USA

⁵Department of Physics, Brown University, Providence, Rhode Island 02912-1843, USA

email: Akusti.Jaatinen@tkk.fi